Energy Equip. Sys./ Vol. 10/No. 3/Sep. 2022/ 287-308

ENERGY EQUIPSYS

Energy Equipment and Systems

http://energyequipsys.ut.ac.ir
www.energyequipsys.com

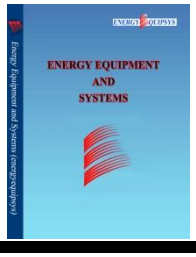

Nanoparticle addition and path-curvature-effect on heat transfer in a typical conical spiral duct with a square cross-section

Authors

Mansour Talebi[a*]
Aliasghar Ghasemi[b]
Afshin Ahmadi Nadooshan[c]

[a] Reactor and Nuclear Safety Research School, Nuclear Science and Technology Research Institute, Iran

[b] Islamic Azad University, Majlesi Branch, Iran

[c] Engineering Faculty, Shahrekord University, Shahrekord, Iran

Article history:

Received : 17 February 2021
Accepted : 4 July 2021

ABSTRACT

A comprehensive study was conducted on how different nano-fluids affect the heat transfer characteristics of a conical spiral duct with a square section. Metallic, non-metallic and Carbon nanotube (CNT) nanoparticles were assumed to be added to water as coolant in the spiral side of heat exchangers. The combined effects of nanoparticle dispersion and path curvature on heat transfer enhancement under two different thermal boundary conditions were investigated. The effects of the flow regime on heat transfer in such a configuration were tested. The flow and energy equations were solved numerically using available commercial software ANSYS FLUENT® Academic Research, Release 16.2. The numerical procedures were verified with available data, and correlation and maximum error were determined to be less than 13%. It was found that compared to the non- curved duct with the same length; heat transfer would increase by about 15%. The addition of metallic nanoparticles also enhanced the heat transfer by 5%. In low Reynolds numbers, crossflow affects temperature distribution and thermal characteristics but in the turbulent regime, the temperature distribution is less sensitive to generated crossflow.

Keywords: Nanofluids, Heat Exchangers, Conical Spiral Ducts, Numerical Heat Transfer.

1. Introduction

Compound techniques of heat transfer enhancement have attracted lots of heat transfer engineers due to their potential to increase the heat transfer rate more than any individual method[1]. Currently, researchers are exploring the potential for different combinations of surfaces and the surrounding fluid. The combinations presented so far could be from amongst different methods such as the active methods (requiring external power to conserve the enhancement mechanism) like fluid stirring, fluid vibration, surface vibration, electromagnetic fields, suction and injection, etc., and the passive methods (not requiring external power to uphold the enhancement characteristics) like: treated surfaces, rough surfaces, extended surfaces, displaced enhancement devices, swirl flow devices, coiled tubes, surface tension devices, additives for fluids, etc.[2].

The combinations which have been studied include Helical-ribbed tube with double twisted tape inserts[3], combined non-uniform wire coil and twisted tape inserts[4], dimpled tube with twisted tape inserts [5], integral type

*corresponding author: Mansour Talebi
Reactor and Nuclear Safety Research School, Nuclear Science and Technology Research Institute, Iran
Email: mansour_talebi@yahoo.com

wall roughness with wavy strip inserts[6], nanofluid with twisted tape insert [7], and helical screw tape coupled with rib tabulators [8]. According to literature data, the use of conical spiral ducts rather than straight ones remarkably improves the heat transfer rate [9-11]. In an experimental study, Pramod et al. [12]investigated conical coils with various cone angles and tube diameters. Hashemian et al. [13] executed a numerical study on multi-criteria analyses in a conical double pipe heat exchanger. Heat transfer characteristics when conical rings were inserted in a round tube were investigated by Anvari et al. [14]. On the other hand, compared with the base fluid flow; nanofluid flows showed an improvement in convective heat transfer rate in various heat transfer systems [15-17]. Muhammad et al. [18]reviewed the use of nanofluid in enhancing the thermal performance of stationary solar collectors. Sun et al. [19] examined the heat transfer characteristics of nanofluids in plate form. An overall analysis of nanofluid flowing through microchannel heat sinks was conducted by Xia et al. [20]. Abbassi et al. [21-22] also studied the effects of using nanofluid in heat removal from a dummy nuclear fuel rod, experimentally and numerically. Finally, it was suggested that when the two enhancing methods are used simultaneously the efficiency of heat transfer gets considerably higher.[23-24]. In this paper, heat transfer enhancements of three different nanofluid flow inside conical ducts were studied numerically under isothermal and constant heat flux boundary conditions. The 3-D simulations with single-phase model for nanofluid flow were run using ANSYS FLUENT® Academic Research, Release 16.2 [25-27].

In these simulations, the effects of a wide range of different parameters such as nanofluid type (nanofluid made by Cu, CuO, and CNT nanoparticles which have good thermal properties), nanofluid volume concentrations (0.5%, 1%, 2% and 4%), flow regime and Reynolds number at different boundary conditions, in a spiral duct were studied. To investigate the effects of fluid type on heat transfer, pure water and nanofluid with volume concentrations of 0.5%, 1%, 2% and 4%, were tested as the working fluid. The thermophysical properties of the working fluid were predicted using available information from previous studies. The conical spiral duct with a square cross-section is used in condensers and evaporators.

Nomenclature

C_p Specific heat [J/kg K]
d_h Hydraulic diameter [m]
h Heat transfer coefficient [W/m^{2}K]
K Thermal conductivity [W/mK]
l Test section length [m]
Nu Nusselt number
P Power [W]
$q"$ Heat flux [W/m^2]
$\dot{q}$ Generated heat [W]
r_{in} Inner tube radius [mm]
Re Reynolds number
T Temperature [K]

Greek Symbols

μ Viscosity [kg/s.m]
ρ Density [kg/m^3]
φ nanoparticles concentration [%]

Indices

f Base Fluid
nf nanofluid
p nanoparticles

2. Methodology

2. 1. Model Geometry

The geometry of a typical conical spiral duct with an attack angle of 70° in association with its dimension is illustrated in Fig. 1. The geometry is based on Sasmito et al. [24] study. They selected the geometry as a microchannel T-junction. There are 3 spiral rounds with a pitch of 60 mm, a larger radius of 250 mm, and a smaller radius of 125 mm. The square cross-section of the model with an edge size of 8mm. The different edges used in this paper are also highlighted.

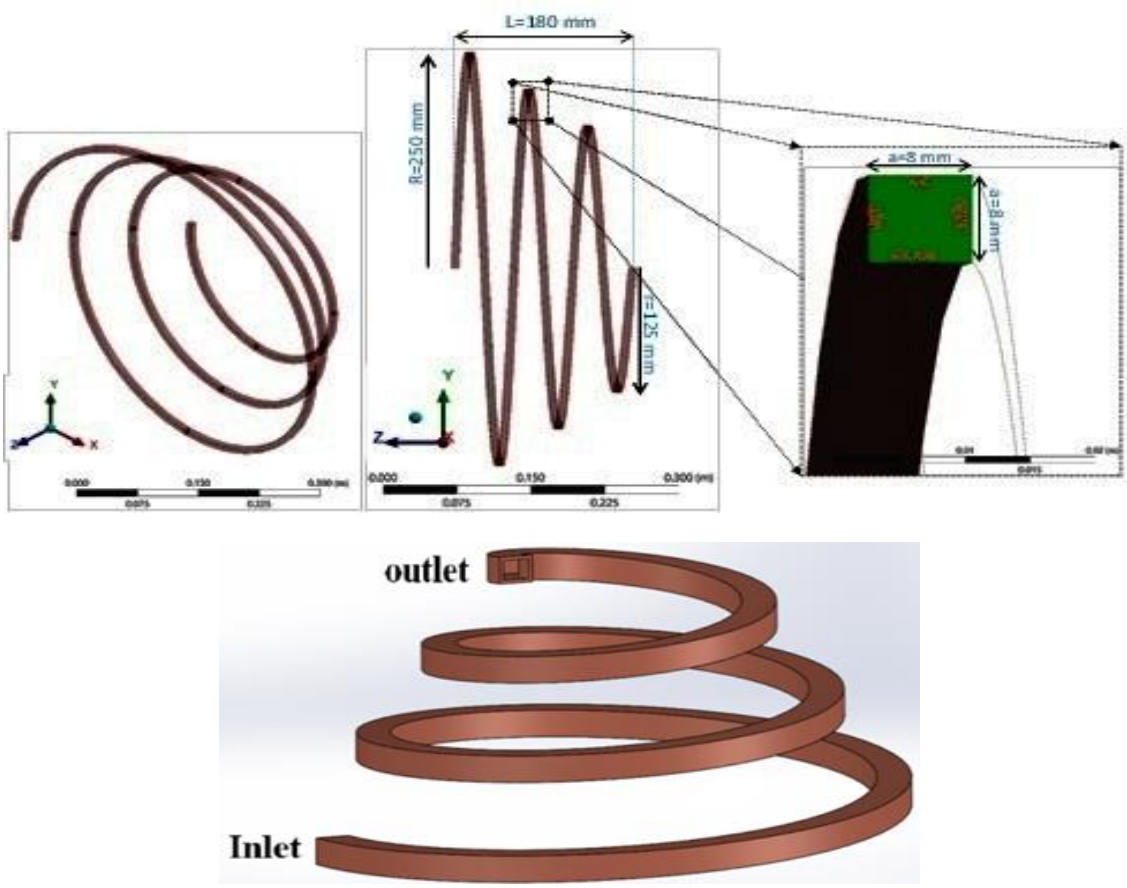

Fig. 1. Schematic diagram under consideration geometry (conical spiral duct with an attack angle of 70°)

2.2. Governing Equations

Single-phase approach was used to model nanoparticle dispersion in the current study. Using modified thermal properties of nanofluids according to the base fluid and nanoparticle characteristics has two advantages: a) The computational cost would be much lesser, and b) the semiempirical correlations are based on experimental data and make lesser uncertainty. Due to the general shape of the spiral cone, the spherical coordinate system was chosen. The two-phase equations for continuity, momentum, and energy in spherical coordinates are given as

continuity:

$$\partial u/\partial z+1/r\left(vr\right)+1/r\ \partial w/\partial\varphi=0 \tag{1}$$

Conservation of momentum:

$$\frac{Dv}{Dt}-\frac{w^2}{r}=-\frac{1}{\rho}\frac{\partial p}{\partial r}+\frac{\mu}{\rho}\left[\nabla^2 w-\frac{v}{r^2}\frac{\partial w}{\partial\varphi}\right] \tag{2}$$

$$\frac{Du}{Dt}=-\frac{1}{\rho}\frac{\partial p}{\partial z}+\frac{\mu}{\rho}\nabla^2 u \tag{3}$$

Conservation of energy:

$$\frac{\partial T}{\partial z}+v\frac{\partial T}{\partial r}+\frac{w}{r}\frac{\partial T}{\partial\varphi}= \left(\frac{k}{\rho c_p}\right)\left[\frac{\partial^2 T}{\partial z^2}+\frac{1}{r}\frac{\partial}{\partial r}\left(r\frac{\partial T}{\partial r}\right)+\frac{1}{r^2}\frac{\partial^2 T}{\partial\varphi^2}\right]+\left(\frac{\mu}{\rho c_p}\right)\Phi \tag{4}$$

where Φ represents the heat dissipation term which is calculated by

$$\Phi=2\left[\left(\frac{\partial u}{\partial z}\right)^2+2\left(\frac{\partial v}{\partial r}\right)^2+\left(\frac{1}{r}\frac{\partial w}{\partial\varphi}+\frac{v}{r}\right)^2\right]+ \left[\frac{1}{r}\frac{\partial u}{\partial\varphi}+\frac{\partial w}{\partial z}\right]^2++\left[\frac{\partial v}{\partial z}+\frac{\partial u}{\partial r}\right]^2+ \left[\frac{1}{r}\frac{\partial v}{\partial\varphi}+\frac{\partial w}{\partial r}-\frac{w}{r}\right]^2 \tag{5}$$

The general thermal-hydraulic features of water nanoparticle solution are functions of the

base fluid and nanoparticle concentration. The density of the solution is calculated by [22]

$$\rho_{nf} = (1-\phi)\rho_{bf} + (\phi)\rho_{np} \tag{6}$$

In this equation b_f and np correspond to water and nanoparticle thermal properties, and ϕ is the volumetric concentration. The specific heat of the solution is given by[22]

$$(C_p)_{nf} = \frac{(1-\phi)(\rho_{bf} C_{p,bf}) + (\phi)(\rho_{np} C_{p,np})}{(1-\phi)\rho_{bf} + (\phi)\rho_{np}} \tag{7}$$

The effective dynamic viscosity of the nanofluid is given by [28]

$$\mu_{nf} = \mu_{nf} + \frac{\rho_{np} V_B d_{np}^2}{72C\delta} \tag{8}$$

where δ and V_B denote the particle's distance and the nanoparticles' Brownian speed, which are, respectively, calculated using[28]

$$V_B = \frac{1}{d_{np}} \sqrt{\frac{18k_B T}{\pi \rho_{np} d_{np}}} \tag{9}$$

and

$$\delta = \sqrt[3]{\frac{\pi}{6\phi}} d_{np} \tag{10}$$

where k_B is Boltzmann constant and α_{bf} is related to the thermal diffusivity of the water. $d_{bf}$and d_{np} stand for molecule size of the base fluid and nanoparticles diameter, respectively, and C is calculated using

$$C = \frac{1}{\mu_{bf}} \left[\left(1133 d_{bf} + 2.771E^{-6}\right) + \left(90 d_{np} + 3.93E^{-7}\right) \right] \tag{11}$$

One should note that the unit of particle size (i.e. d_{np}) is m in all equations.

The model used for thermal conductivity was a temperature-dependent one, in which the Brownian motion is also taken into consideration [29] Thus

$$\frac{k_{nf}}{k_{bf}} = 1 + 64.7\varphi^{0.7466} \left(\frac{d_{bf}}{d_p}\right)^{0.3690} \left(\frac{k_{np}}{k_{bf}}\right)^{0.7476} \left(\frac{2.74E^{-5} \times 10^{\frac{274}{T-140}}}{\rho_{bf}\alpha_{bf}}\right)^{0.9955} \left(\frac{\rho_{bf} k_B T}{3\pi \left(2.74E^{-5} \times 10^{\frac{274}{T-140}}\right)^2 l_{bf}}\right)^{1.2321} \tag{12}$$

where l_{bf} is the mean free path of the base fluid, and is 0.17 (nm) for water.

2.3. Heat Transfer Analysis

Due to the small size of the nanoparticles and the thermal equilibrium condition, it is assumed that the nanoparticles are easily dispersed in the base fluid, and thus the nanofluid assumed a single-phase homogeneous fluid with physical properties based on the concentration of the two components.

Therefore, the basic equations can be generalized to the nanofluid, except that the effective properties of the nanofluid should be replaced by the base fluid properties.

Two different thermal boundary conditions are applied on the surface of the conical spiral duct, namely the constant heat flux boundary condition ($q" = 10000\ [W/m^2]$) and isotherm boundary condition ($T_s = 308\ [°K]$). The mean temperature of the fluid entering the duct is given as $T_i = 298.15\ [°K]$. The mean temperature in any cross-section normal to the flow is calculated according to a mass-weighted average base as

$$T_m = \frac{\int_{A_c} \rho c_p T u dA_c}{\int_{A_c} \rho c_p u dA_c} \tag{13}$$

where A_c is the cross-section area, T is the temperature distribution in the cross-section, u is the velocity normal to the Ac, $\rho$is the density and Cp is the specific heat of fluid. These two parameters are assumed to be constant in the cross-section. The local convection heat transfer coefficient is calculated as

$$h = \frac{-\frac{\partial T}{\partial n}\Big)_{n=0}}{T_s - T_m} \tag{14}$$

In this equation T_s is the surface temperature, T is the temperature distribution, and n represents the vertical distance from the wall surface. The local Nusselt number is also calculated as

$$Nu = \frac{hD_h}{k} \tag{15}$$

where k represents the thermal conductivity of fluid and D_h are the hydraulic diameter of the duct and is calculated as

$$D_h = 4A_c / p \tag{16}$$

where p is the perimeter of A_c.The convection heat transfer coefficient in the isothermal surface boundary condition can be calculated as

$$\dot{Q} = \dot{m}c_p\left(T_e - T_i\right) = \bar{h}A_s\left(T_s - T_m\right)_{avg} = \bar{h}A_s\Delta T_{lm} \tag{17}$$

In this equation $\bar{h}$ is the average value of heat transfer coefficient in duct surface, and A_s which is calculated by Computational fluid dynamics (CFD). The mean logarithm temperature in this equation is calculated by

$$\Delta T_{lm} = \frac{T_i - T_e}{ln\left[\left(T_s - T_e\right)/\left(T_s - T_i\right)\right]} \tag{18}$$

where T_i and T_e are the inlet and outlet mean temperatures, respectively. In constant heat flux boundary conditions, the rate of heat transfer is known and the duct surface temperature has to be calculated. Using the numerical method, the average heat transfer coefficient and duct surface temperature can be calculated as

$$\dot{Q} = \bar{h}A_s\left(T_s - T_m\right) \tag{19}$$

Because the mass flow and cross-section are constant along the fluid flow, the Reynolds number is constant for each case. For this study Re_C is about 1000 [34].

2.4. Pressure Drop

Pressure drop in the conical spiral is determined by calculating the average pressure in the outlet and inlet. The head pressure drop is obtained from the following equation:

$$h_L = \frac{\Delta P_L}{\rho g} = f\frac{L}{D}\frac{V_{avg}^2}{2g} \tag{20}$$

Where V_{avg} is the average velocity in A_c cross-section. Due to vortices and radial motion of the fluid, a localized pressure drop occurs. But in this study, numerical methods were used to obtain pressure drop.

3. Results and Discussion

Structured hexahedral cells are used for the grid. The inflation is applied at the wall boundaries to capture adequate y-plus (Fig. 2). The Quick method, SIMPLE algorithm, and *k-ε* model were manipulated. The value of y+ is greater than 30 and lesser than 100, and hence the standard wall function could be applied.

Table 1. nanoparticle properties

nanoparticle	Density (kg/m^3)	Specific heat (J/K)	Thermal conductivity (W/m^{2}K)
CuO	6510	540	18
Cu	8933	385	401
CNT	2600	425	3000

Table 2. Comparison of literature and experimental results [33-34]

Geometry and cross-section	$f.Re$ $Re = 400$		$Error$%	Nu $q'' = constant$		$Error$%	Nu $Ts = Constant$		$Error$%
	References & equations	This study		References & equations	This study		References & equations	This study	
Straight pipe	16.0	16.3	1.8%	4.364	4.85	10.0%	3.66	4.00	8.5%
Straight duct	14.2	14.6	2.7%	3.63	4.1	11.5%	2.89	3.32	13.0%
Conical spiral pipe	21.7	22.8	4.8%	11.44	12.9	11.3%	10.32	11.48	10.1%
Conical spiral duct	Not mentioned	19.1	-	Not mentioned	10.5	-	Not mentioned	8.02	-
				Nu (Re=4000, CNT, $\emptyset = 0.5\%$, $q'' = constant$)					
Cone Helical Coiled Tube (CNT)				References & equations 55.2			This study 56.8		

In order to verify the computational procedure, the simulation was done for straight rectangular ducts and pipes in addition to conical spiral ducts and pipes [33] and cone helical coiled tubes [34]. Obtained Nusselt numbers and pressure drop values were compared to literature values and the results are tabulated in Table 2. Due to the error values presented in Table 2, the errors in the results of this research are the same. The Nusselt number for straight pipes and ducts in fully developed and developing regions exists in most standard heat transfer textbooks [30-31]. In the case of conical spiral pipes, the results of this numerical solution were compared to the empirical equation developed by Manlapaz-Churchill [32-33] for helical coils. The Manlapaz-Churchill equation for constant heat flux condition is given as

$$Nu_H = \left[\left(4.364 + \frac{4.364}{\left(1+\frac{1342}{De^2 Pr}\right)^2} \right)^3 + 1.816 \left(\frac{De}{1+\frac{1.15}{Pr}} \right)^{\frac{3}{2}} \right]^{\frac{1}{3}} \quad (21)$$

The corresponding equation for the isothermal boundary condition is given as

$$Nu_T = \left[\left(3.657 + \frac{4.343}{\left(1+\frac{957}{De^2 Pr}\right)^2} \right)^3 + 1.158 \left(\frac{De}{1+\frac{0.477}{Pr}} \right)^{\frac{3}{2}} \right]^{\frac{1}{3}} \quad (22)$$

The pressure drop is calculated as

$$\frac{f_c}{f_s} = \begin{cases} 1 & De < 30 \\ 0.419 De^{0.275} & 30 < De < 300 \\ 0.1125 De^{0.5} & De < 300 \end{cases} \quad (23)$$

In these equations, Pr is the Prandtl number of coolant, Nu_H is the Nusselt number for constant heat flux boundary condition, Nu_T is the Nusselt number for constant temperature boundary conditions, f_c is the friction factor for curved pipe, f_s is the friction factor for straight pipe, and De is the Dean number, which represents the curvature of the path and is defined as

$$De = Re \left(\frac{D_h}{2R} \right)^{\frac{1}{2}} \quad (24)$$

where Re is the Reynolds number, D_h is the hydraulic diameter of the duct cross-section and R is the radius of curvature. The values of D_h equal to a in Fig. 1.

For numerical simulation, the second-order upwind scheme decoupling with the SIMPLEC algorithm is used, and governing equations are solved by a finite volume method.

In order to study the dependency of mesh, various element size was examined. The effect of the number of grids on the Nusselt number is depicted in Fig. 3. Eventually, the grid with 1.5E6 cells was selected. The x, y and sweep divisions are 50 and 60 respectively. The ratio between the smallest cell to the largest one in the x and y direction is 10 to ensure the desired y+. It can be seen that under the worst conditions, the error does not exceed 13%. The Nusselt number and friction factor in squared ducts are smaller than the values in circular tubes. According to the definition of the Nusselt number, this will result in a smaller heat transfer coefficient, but because there is a larger heat transfer area in squared ducts, the total heat transfer would be higher in equal conditions.

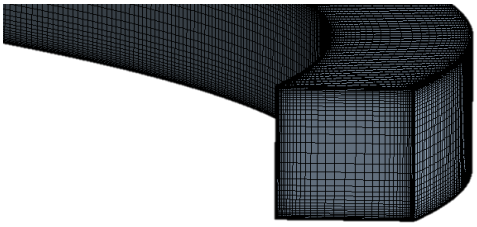

Fig. 2. Grid Representation

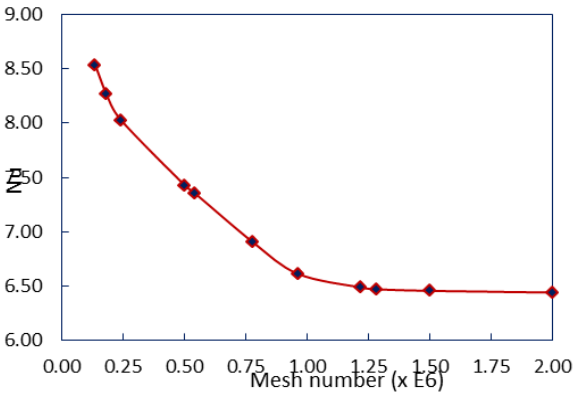

Fig. 3. Mesh Independency Criteria

3.1. Effects of curvature on temperature distribution

The difference between curved ducts and straight ducts is the formation of secondary flow (crossflow). The strength and shape of the cross-flow may affect the heat transfer rate and temperature distribution. Fig. 4, illustrates the cross-flow vectors, velocity contours, and temperature distribution contours for the isothermal boundary condition and the constant heat flux boundary condition. The cross-section location in the duct is highlighted in Fig. 1.

In order to make a comparison, the contours are presented for a conical spiral duct (Figure 1) and a straight duct with equal length. The cross-section of contours in the straight duct is placed at the same length as that of the conical spiral duct in Fig. 1. Since there is no crossflow in a fully developed flow in a straight duct, the cross-flow vectors and contours are not presented in Fig. 4. In both turbulent and laminar flow in the straight duct, there is a region in the middle of the section which represents a high velocity and high-temperature region.

These regions have similar circular shapes and coincide with each other. In addition to crossflow, velocity contours vary in comparison to the straight pipe. This is mostly because of centrifugal forces which deviate from the high-velocity region to be in the same proximity as the top edge of the section. In turbulent flow, the temperature distribution approximately follows the velocity contours, and the cold region coincides with the high-velocity region and has the same shape.

This is not the case in laminar flow, as the cold region (in both boundary conditions) and the high-velocity region do not coincide and do not have the same shape. In fact, there are 2 cold regions in laminar flow. By taking a look at the crossflow contours, it seems that the two cold regions coincide with the region in which the crossflow vectors are a maximum. In other words, the crossflow has an impact on temperature distribution in laminar flow but it is less effective in a turbulent flow.

In the isothermal condition, the area of the cold region in the curved pipe is smaller than that in the straight pipe. This happens in both laminar and turbulent regimes. One could conclude that the curvature of the duct could improve the heat transfer rate. In laminar flow, it could be observed that the temperature gradient increased on the top, right and left edges but decreased on the bottom edges. The convection heat transfer coefficient in the bottom edges is lower than that on the other edges. These phenomena are more obvious in laminar flow than in turbulent flow regime.

On the other hand, in constant heat flux condition, the wall averaged temperature in the curved duct is obviously lower than that of the straight duct. As the other boundary condition, in the constant heat flux condition, the curvature has a more brilliant effect in laminar flow in comparison with turbulent flow.

3.2. Effect of nanofluid on temperature distribution (Qualitative Results)

In this section, the effect of different nanoparticles and their concentration on temperature distribution in laminar and turbulent flow regimes for the isothermal and constant heat flux boundary conditions are presented. in Figs. 5-8. The right column represents flow with CNT nanoparticles, the middle column is related to Cu nanoparticles and the left column represents CuO nanoparticle dispersion. The figures illustrate the temperature contour related to the section highlighted in Fig. 1. As mentioned in the previous section, the temperature distribution profile is dependent on the flow regime.

Fig. 5, illustrates the effects of three different nanofluid concentrations on temperature distribution in Re=400 and the isothermal boundary condition. An increase in nanoparticle concentration in each nanofluid results in a decrease in the cold region area; this implies that the total temperature of the section has increased. The increment for CuO/Water nanofluid is more intense than others.

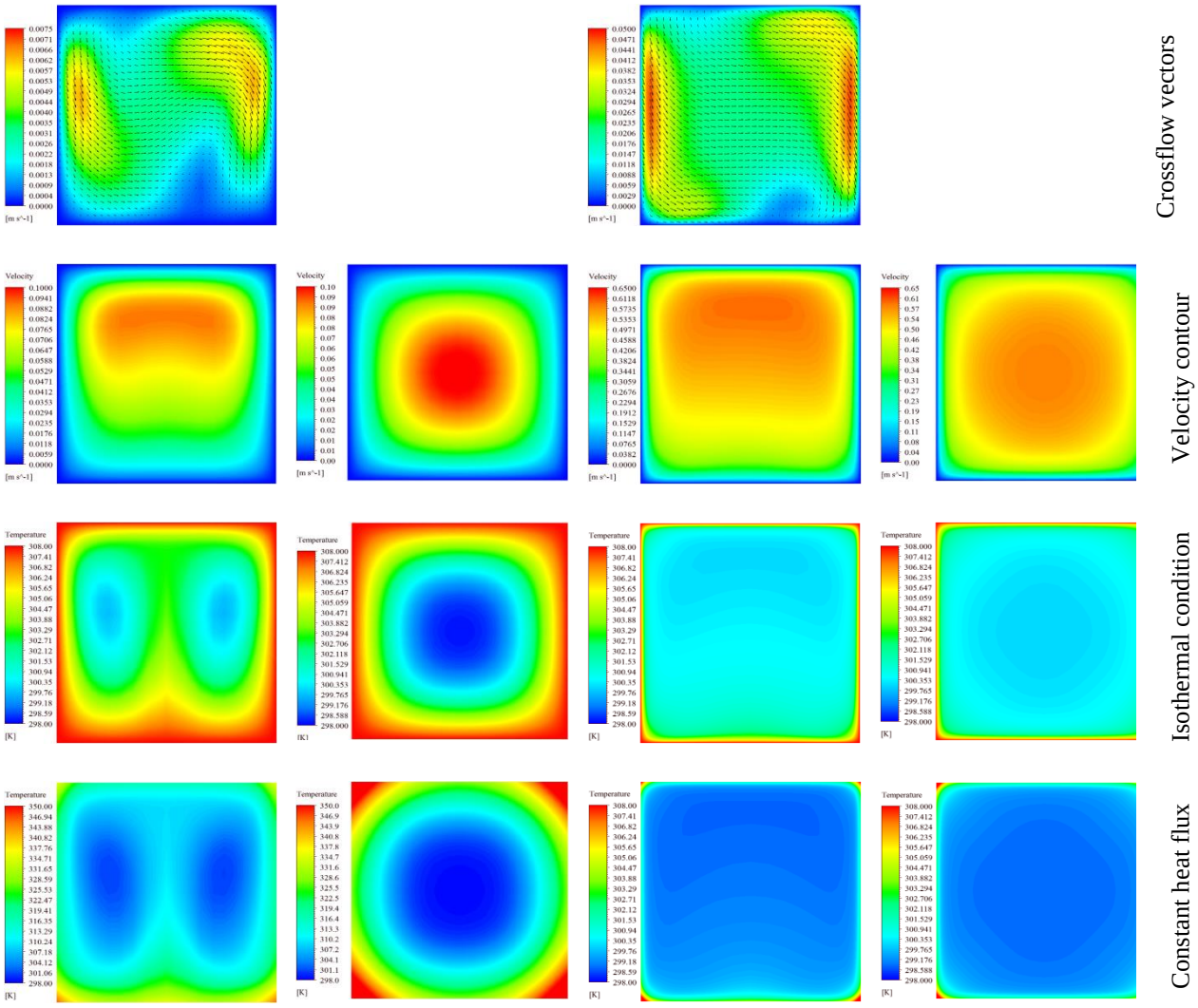

Fig. 4. Comparison between crossflow, velocity contours, and temperature distribution (constant heat flux condition and isothermal condition) in laminar and turbulent regimes

Figure 7, illustrates the effects of three different nanofluid concentrations on temperature distribution in Re=3600 and the isothermal boundary condition. An increase in nanoparticle concentration in each nanofluid results in a decrease in the cold region area. This implies that the total temperature of the section has increased. The increment for Cu/Water nanofluid is more intense than others.

Figure 8, illustrates the effects of three different nanofluids on temperature distribution in Re=3600 and constant heat flux boundary condition. By the addition of nanoparticles in each nanofluid, the area of the cold region would be developed, which results in enhancement of the averaged section temperature. The increment for Cu/Water nanofluid is more intense than others.

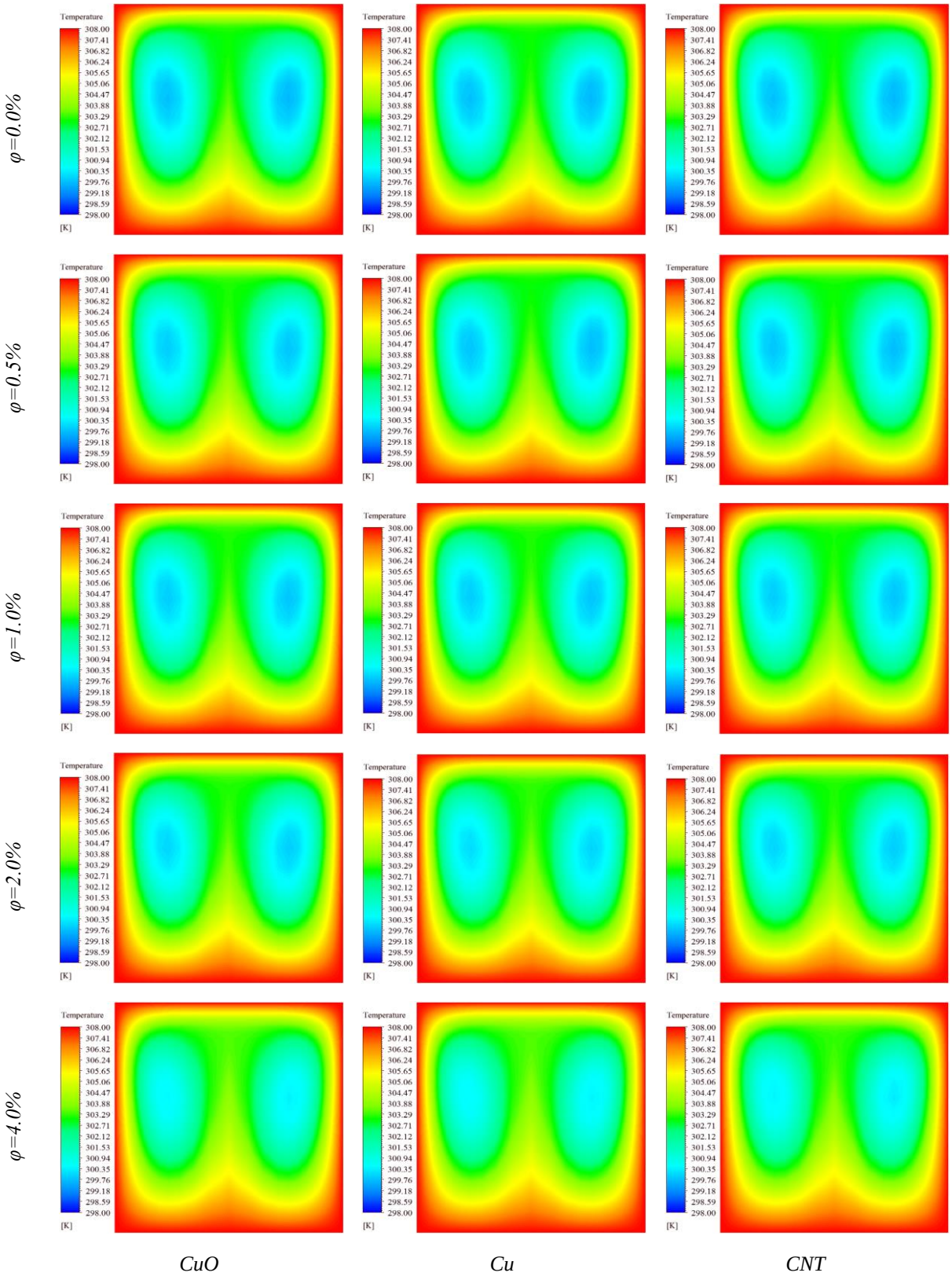

Fig. 5. Effect of different nanoparticle concentrations on temperature distribution in Re=400 and isothermal boundary condition

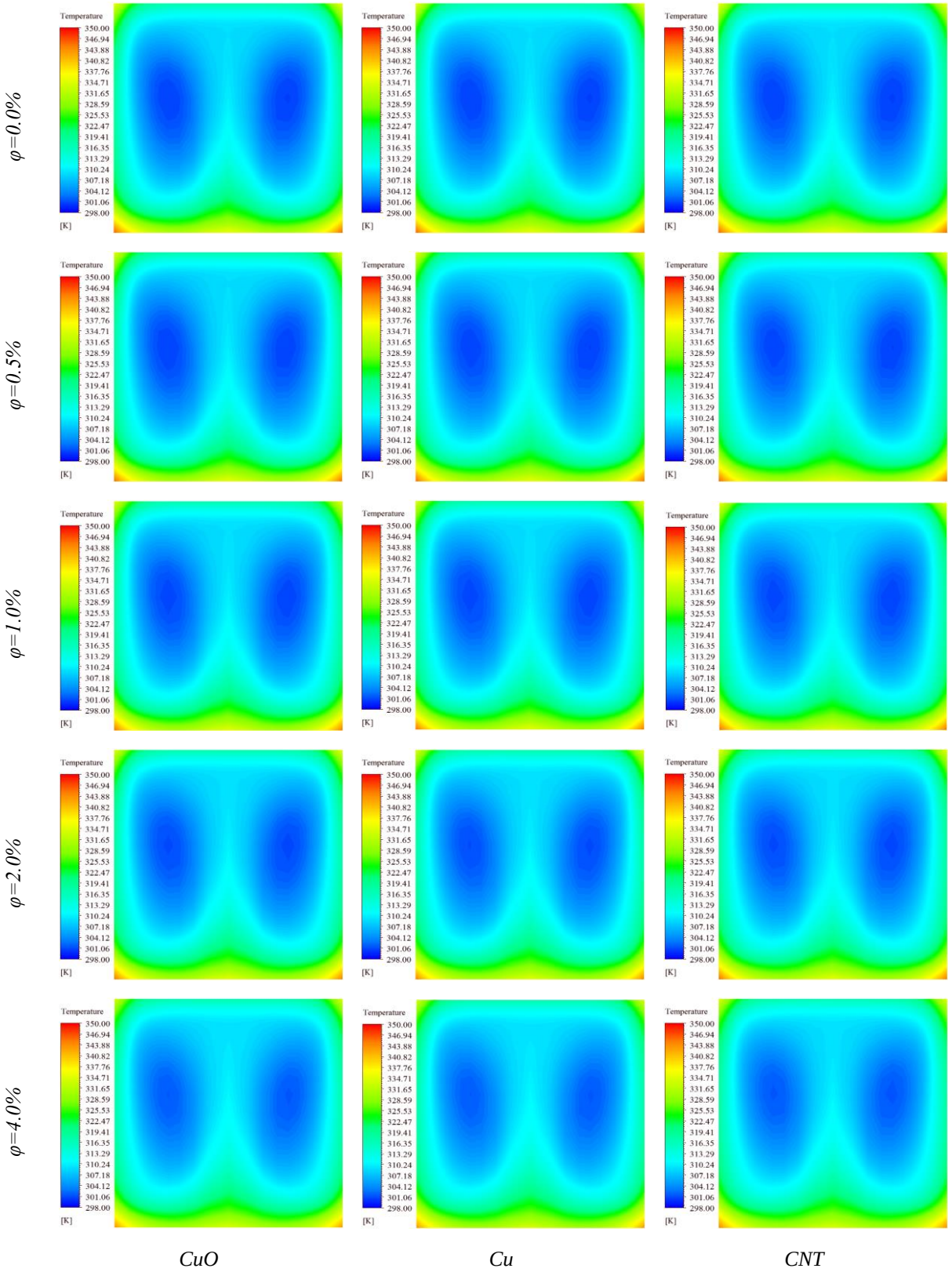

Fig. 6. Effect of different nanoparticle concentrations on temperature distribution in Re=400 and constant heat flux boundary condition

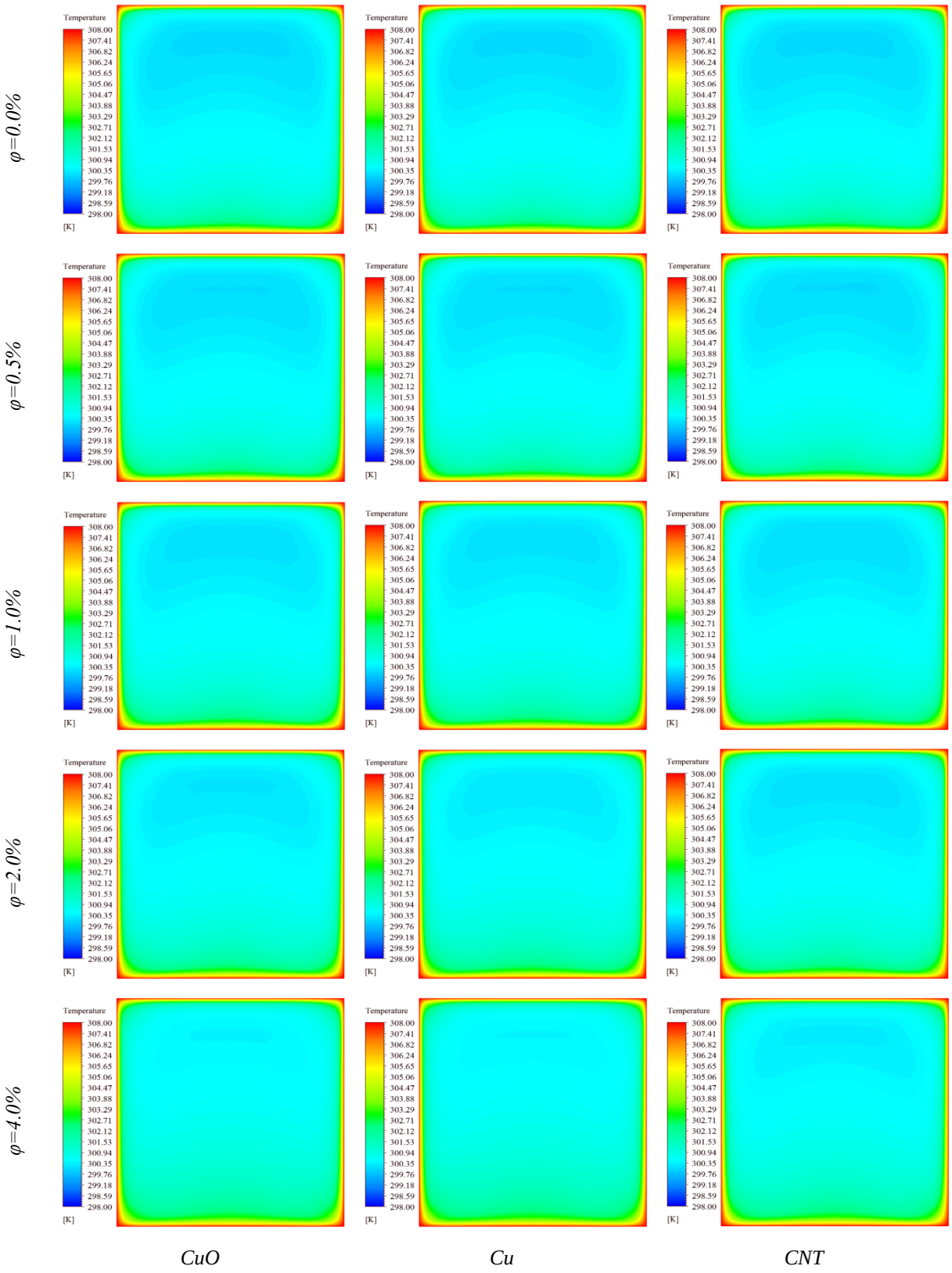

Fig. 7. Effect of different nanoparticle concentrations on temperature distribution in Re=3600 and isothermal boundary condition

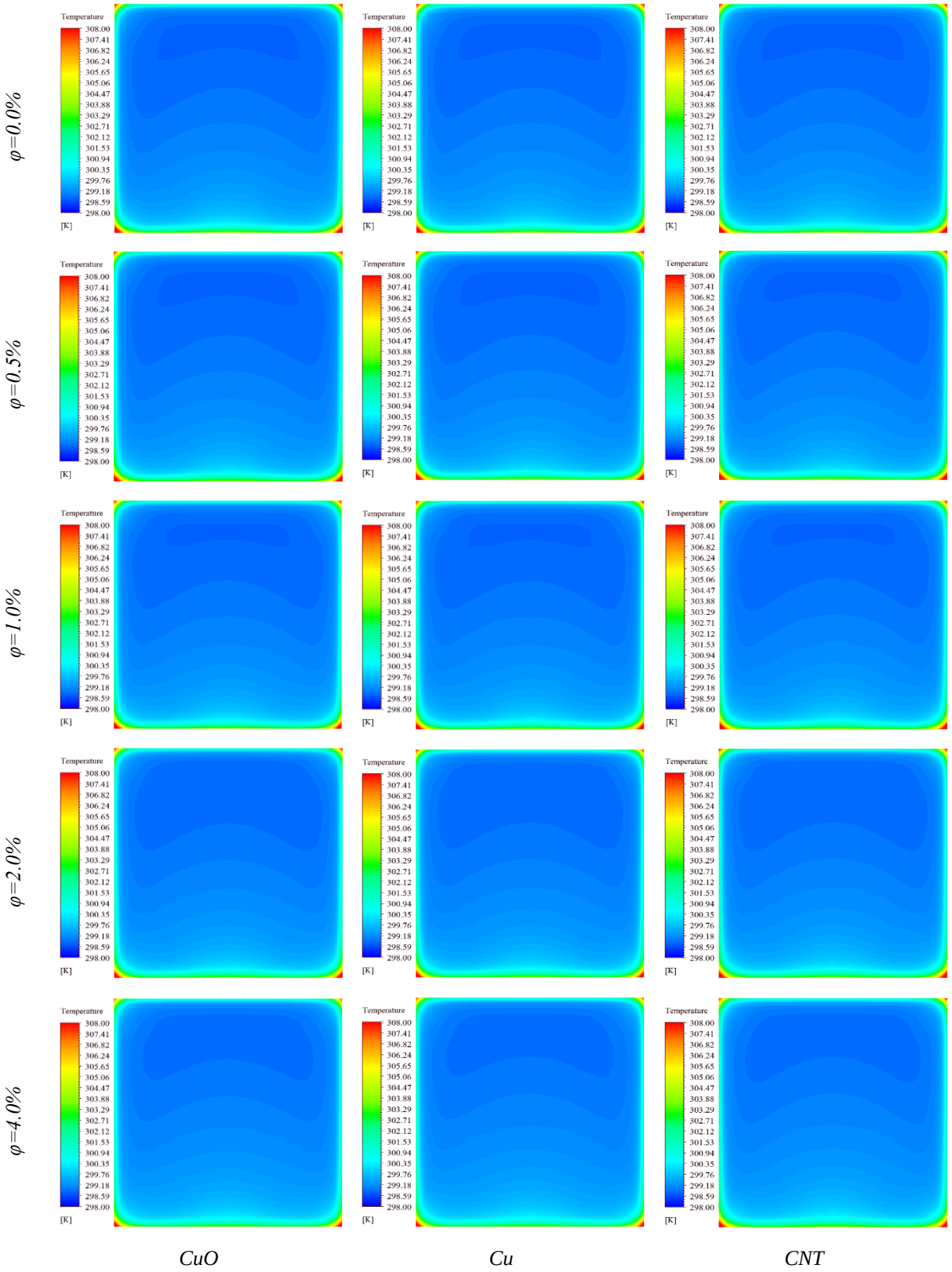

Fig. 8. Effect of different nanoparticle concentrations on temperature distribution in Re=3600 and constant heat flux boundary condition

3.3. Quantitative Results

In the following sections, the effects of different parameters such as flow rate, nanoparticle concentration, etc. would be considered according to the averaged results. Appropriate charts illustrating the effects of different parameters on heat transfer quantities are presented. Some charts present the improvement percentage of nanofluid (with different concentrations) relative to water in the conical spiral duct. The improvement percentage for quantity x is calculated as

$$improvement = 100 \times \frac{x_n - x_w}{x_w} \tag{25}$$

where n represents nanoparticles and w represents water.

The diagrams illustrate the averaged convective heat transfer coefficient and averaged heat addition rate in the isothermal boundary condition; the averaged convective heat transfer coefficient and averaged wall temperature in constant heat flux condition, and pressure drop per unit of length in the geometry under consideration.

3.3.1. Convection heat transfer and heat transfer rate in an isothermal boundary condition

Figure 9.a, illustrates the effect of nanoparticle concentration on heat transfer coefficients for three different nanofluids in the isothermal boundary condition. It could be observed that the addition of nanoparticles would enhance the convective heat transfer coefficient in all three nanofluids.

The increment slope is higher in higher concentrations. However, the increment is more severe in turbulent flows than in the laminar regime. Fig. 9.b, reveals the improvement percentage for different concentrations in comparison to water which is calculated according to equation 24. It could be stated that for all nanofluids, enhancing nanoparticle concentration would increase the heat transfer coefficient. This improvement in heat transfer is more intense for Cu/Water nanofluid. The nanoparticle would perform better in laminar flow in the isothermal boundary condition and would increase the heat transfer coefficient more than turbulent flow. It could be observed that by increment in nanoparticle concentration up to 4%, the heat transfer coefficient would increase by 10%, 14%, and 8% for CuO/water, Cu/Water, and CNT water, respectively. The improvement percent is less sensitive to Reynolds number in CuO/water nanofluid and very sensitive to Reynolds number for Cu/Water nanofluid.

Figure 10.a, illustrates the effect of nanoparticle concentration on rate of heat transfer from wall for CuO/water, Cu/Water and CNT/water nanofluid in the isothermal boundary condition. It could be detected that when nanoparticles are added, the rate of heat transfer but it is very low in comparison to the amount of heat transfer. In other words, according to Fig. 10.b, the improvement percentage for different concentrations in comparison to water which is calculated according to equation (24), is less than 5%. It could be inferred that for all nanofluid, enhancing nanoparticle concentration would result in increment of heat transfer rate.

This improvement in heat transfer is more intense for Cu/Water nanofluid. The nanoparticle would perform better in laminar flow in the isothermal boundary condition and would increase the heat transfer rate more than in turbulent flow. It could be observed that by increment in nanoparticle concentration up to 4%, the heat transfer rate would increase by 4%, 5.5%, and 1.8% for three different nanofluids, respectively. The improvement percent is less sensitive to Reynolds number in CNT/water nanofluid and very sensitive to Reynolds number for CuO/Water and Cu/Water nanofluid.

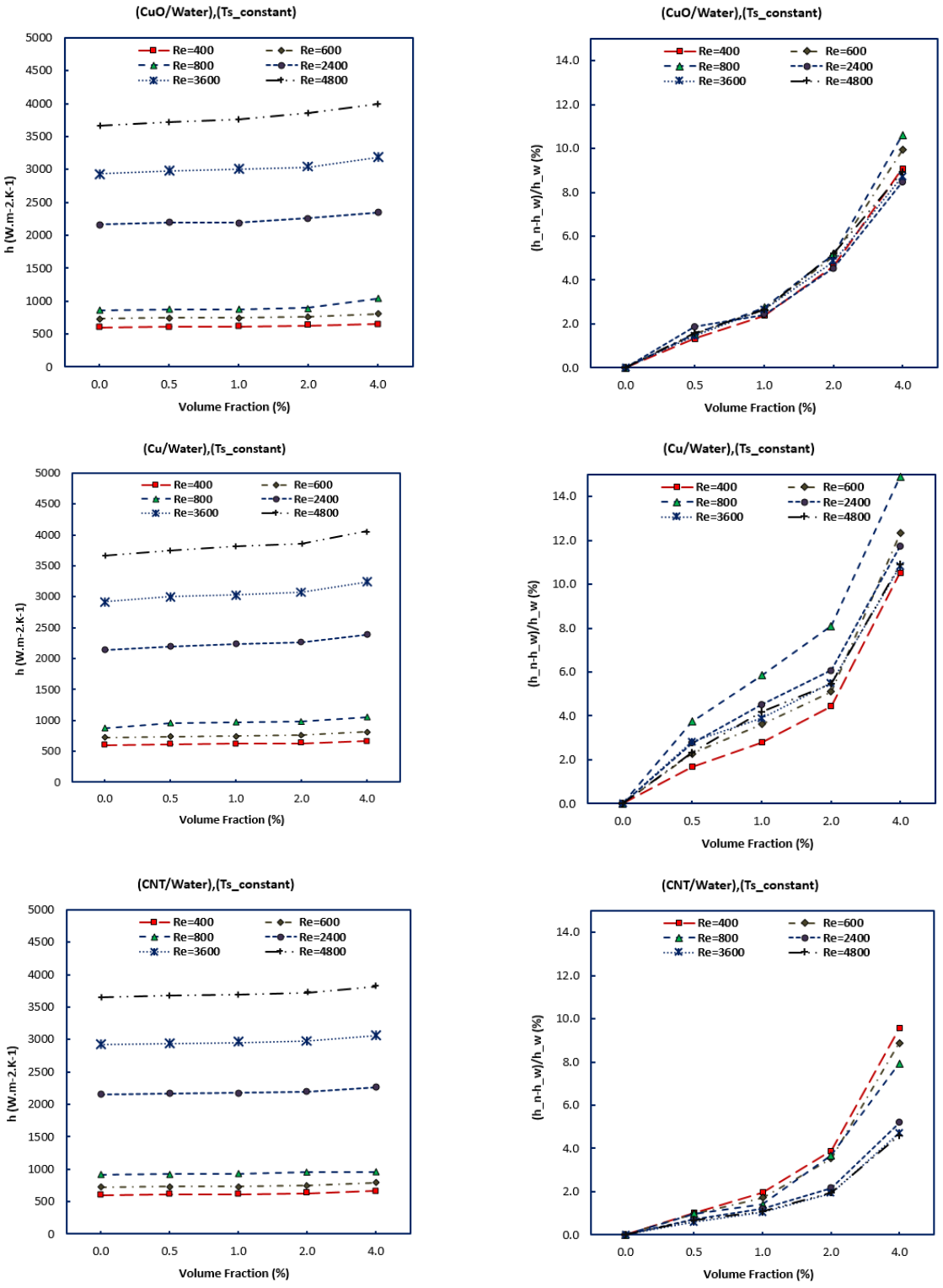

Fig. 9. Effect of CuO, Cu, and CNT nanoparticle concentration and flow velocity on convective heat transfer coefficient inside the conical spiral duct in isothermal boundary condition; a) effect of nanofluid concentration; b) improvement percentage in comparison to water for different concentrations.

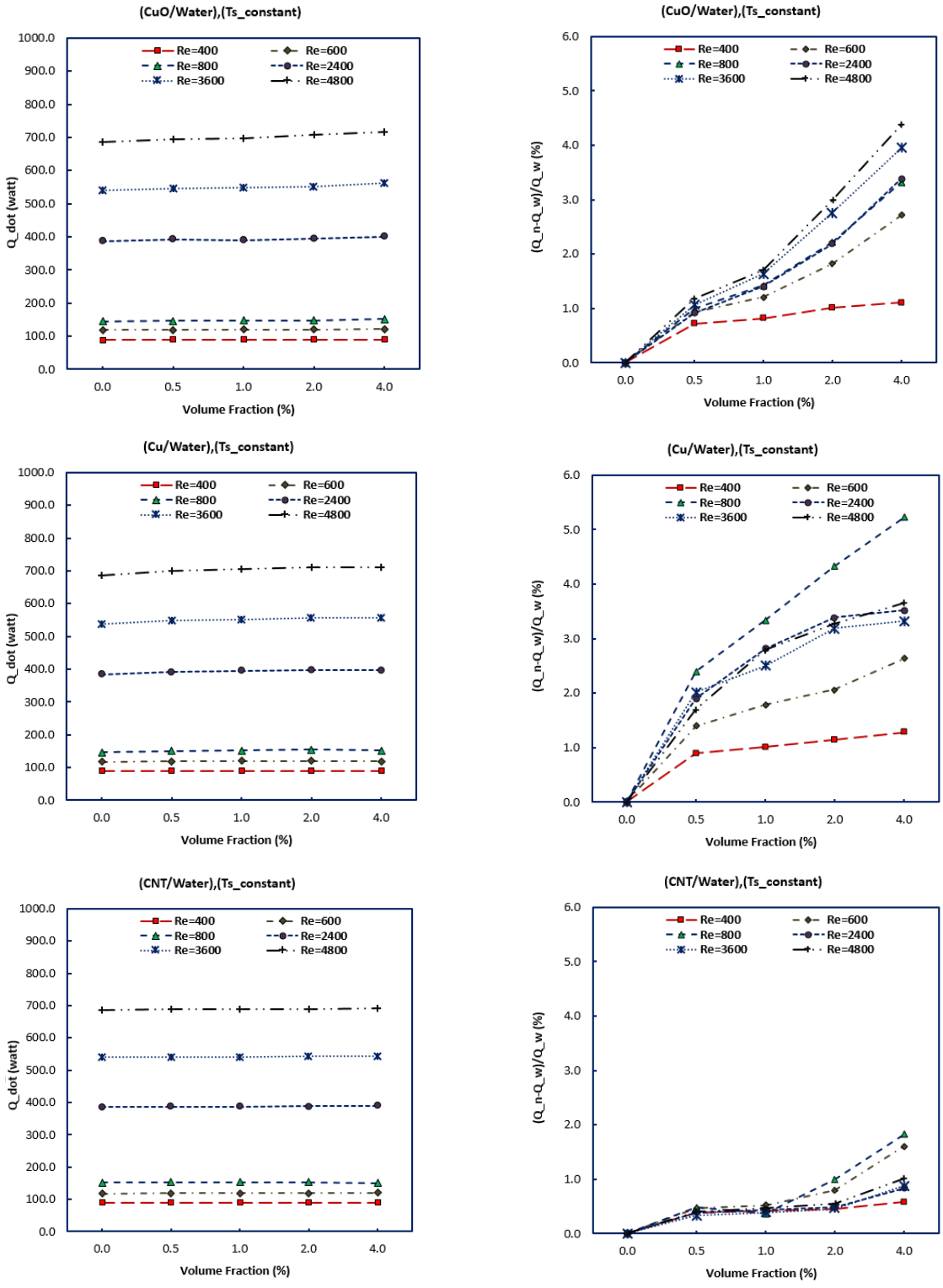

Fig. 10. Effect of CuO, Cu, and CNT nanoparticle concentration and flow velocity on heat transfer rate inside the conical spiral duct in isothermal boundary condition; a) effect of nanofluid concentration; b) improvement percentage in comparison to water for different concentrations.

3.3.2. Convection heat transfer and surface temperature in constant heat flux condition

Figure 11.a, shows the effect of nanoparticle concentration on heat transfer coefficient for CuO/water, Cu/Water and CNT/water nanofluid in the constant heat flux boundary condition. It could be observed that the addition of nanoparticles would enhance the convective heat transfer coefficient in all three nanofluids. The increment slope is higher in higher concentrations. However, the increment is more severe in turbulent flows than in the laminar regime. Fig. 11.b, reveals the improvement percent for different concentrations in comparison to water which is calculated according to equation (24). It could be announced that for all nanofluids, enhancing nanoparticle concentration would increase the heat transfer coefficient. This improvement in heat transfer is approximately similar in all the three nanofluids considered. The nanoparticle would perform better in laminar flow in the constant heat flux boundary condition and would increase the heat transfer coefficient more than that in a turbulent flow. It could be observed that by increment in nanoparticle concentration up to 4%, the heat transfer coefficient would increase by 14%, 18%, and 15.5% for CuO/water, Cu/Water, and CNT water, respectively. The improvement percentage is less sensitive to Reynolds number in Cu/water nanofluid and very sensitive to Reynolds number in CNT/Water nanofluid.

Figure 12.a, illustrates the effect of nanoparticle concentration on the temperature of the conical spiral wall for CuO/water, Cu/Water and CNT/water nanofluid in the constant heat flux boundary condition. It could be observed that the addition of nanoparticles would reduce the temperature of the wall in all three nanofluids. The reduction slope is higher in higher concentrations. However, the reduction is more severe in turbulent flows than in the laminar regime. Fig. 12.b, reveals the improvement percentage for different concentrations in comparison to water which is calculated according to equation (24). It could be announced that for all nanofluids under consideration, enhancing nanoparticle concentration would result in a reduction in the wall temperature. This improvement in heat transfer is more severe in Cu/Water and CuO/water nanofluid compared with CNT/Water nanofluid. The nanoparticle would perform better in laminar flow in the constant heat flux boundary condition and would decrease the wall temperature more than that in a turbulent flow. It could be observed that by increment in nanoparticle concentration up to 4%, the wall temperature decreases by7.5%, 8%, and 3.5% for CuO/water, Cu/Water, and CNT water, respectively. The improvement percentage is less sensitive to Reynolds number in CNT/water nanofluid and very sensitive to Reynolds number for CuO/Water nanofluid.

3.3.3. Pressure drop

Figure 13.a, illustrates the effect of nanoparticle concentration on pressure drop per unit length in the conical spiral wall for CuO/water, Cu/Water and CNT/water nanofluid. It could be observed that the addition of nanoparticles would increase pressure drop. The reduction slope is higher in higher concentrations. However, the reduction is more severe in turbulent flows than in the laminar regime.

Figure 13.b, reveals the improvement percent for different concentrations in comparison to water which is calculated according to equation 24. It could be announced that for all three nanofluids, enhancing nanoparticle concentration would increase the pressure drop. This enhancement in pressure drop has a similar trend in Cu/Water, CNT, and CuO/water nanofluid.

The nanoparticle would cause more pressure drop in turbulent flow than in laminar flow. It could be observed that by increment in nanoparticle concentration up to 4%, pressure drop would increase by 17%, 24%, and 10% for CuO/water, Cu/Water, and CNT water, respectively. In the low Reynolds numbers, the pressure drop is less sensitive to the nanoparticle concentration.

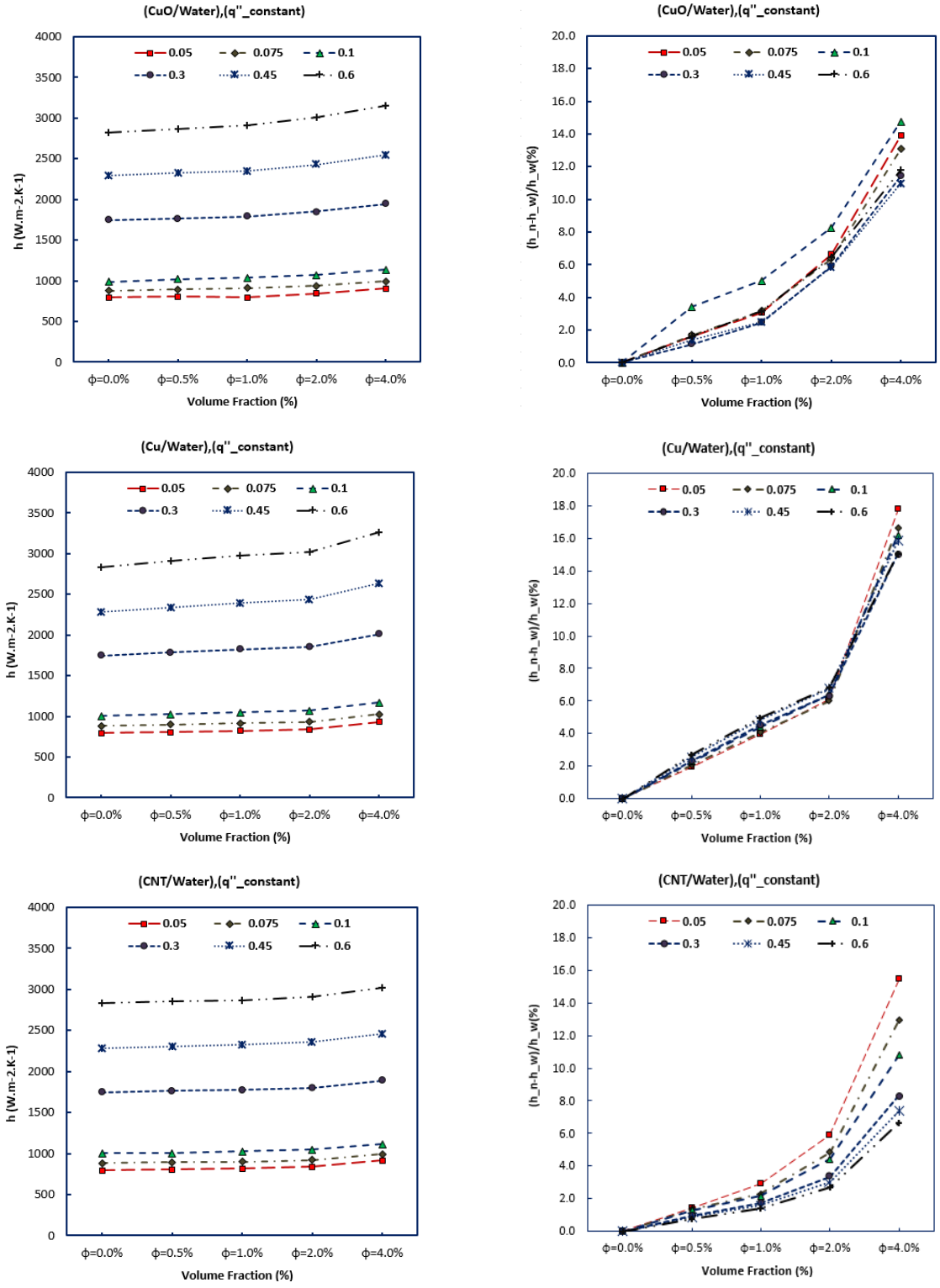

Fig 11. Effect of CuO, Cu, and CNT nanoparticle concentration and flow velocity on convective heat transfer coefficient inside the conical spiral duct in constant heat flux boundary condition; a) effect of nanofluid concentration; b) improvement percentage in comparison to water for different concentrations.

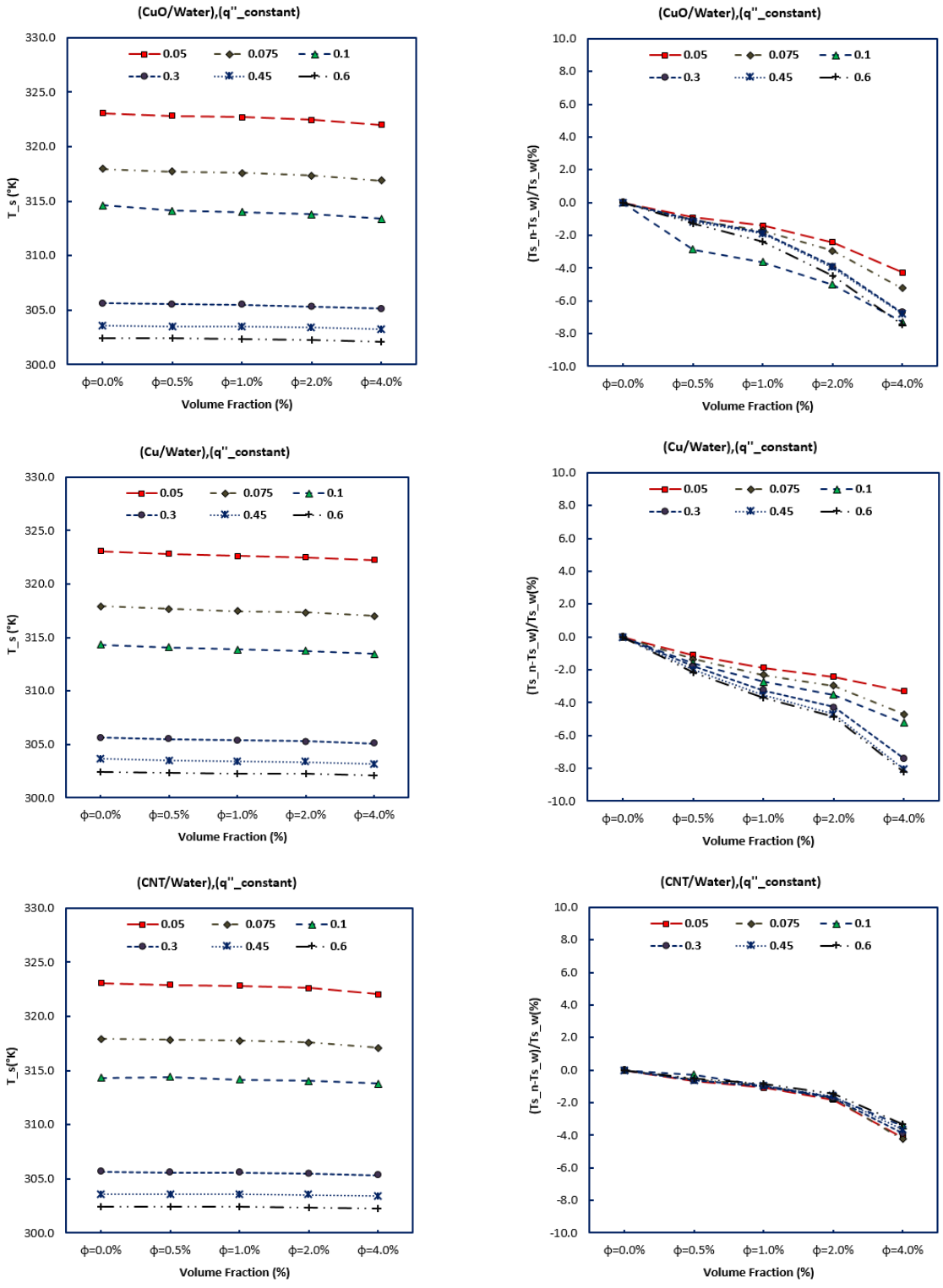

Fig 12 Effect of CuO, Cu, and CNT nanoparticle concentration and flow velocity on the temperature of the conical spiral wall in constant heat flux boundary condition; a) effect of nanofluid concentration; b) improvement percentage in comparison to water for different concentrations.

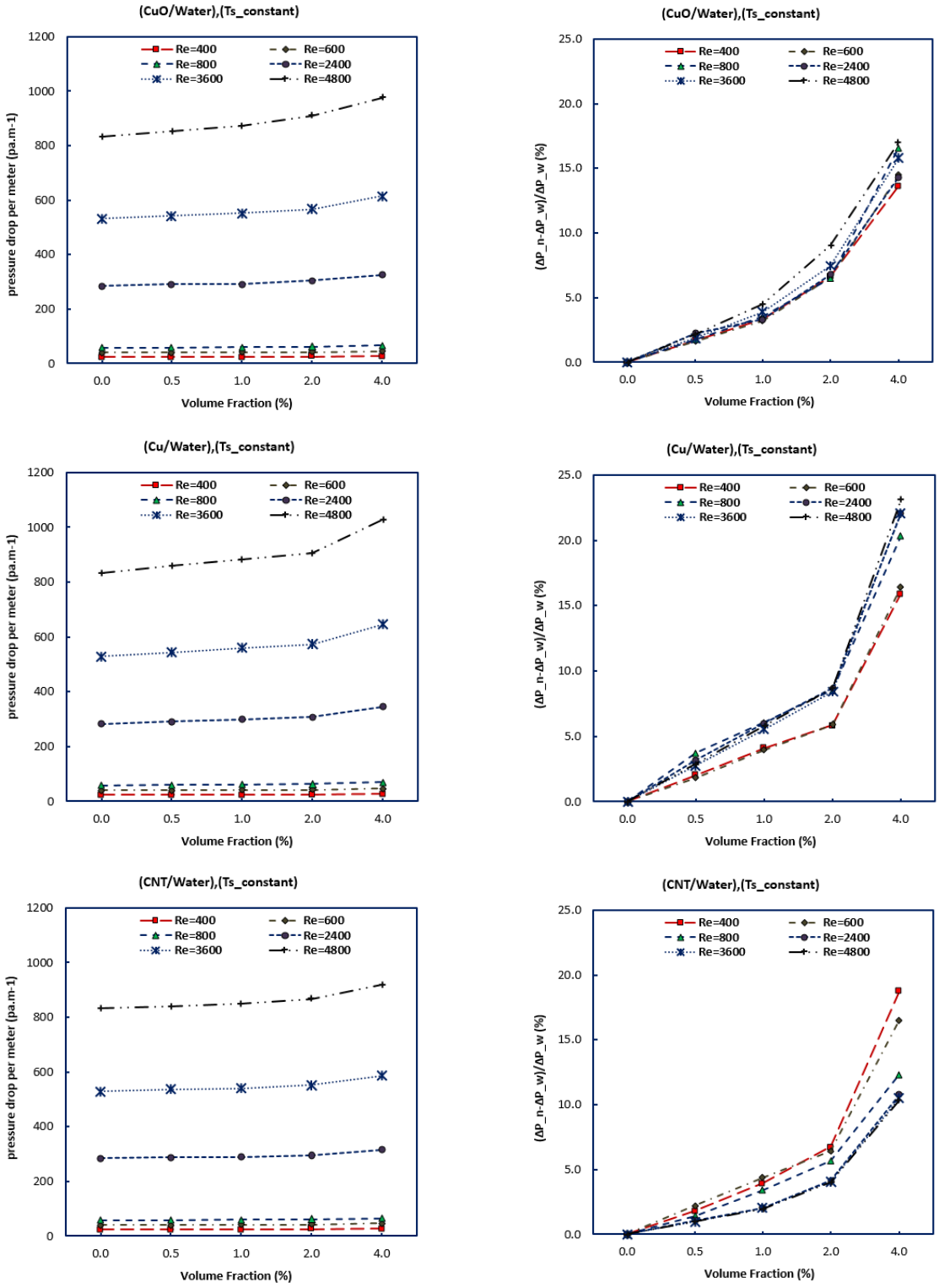

(a) (b)

Fig. 13. Effect of CuO, Cu, and CNT nanoparticle concentration and flow velocity on pressure drop of the conical spiral wall in constant heat flux boundary condition; a) effect of nanofluid concentration; b) improvement percentage in comparison to water for different concentrations.

4. Conclusion

The thermal-hydraulic characteristics of a typical conical spiral duct (attacking angle of 70°) under different boundary conditions, with different nanofluids as coolants are presented in this paper.

Combined effects of path curvature and essence of nanoparticles as two passive methods of heat transfer enhancement were analyzed numerically. The study concludes that:

- In the constant heat flux boundary condition and Re=400, if a straight squared duct is placed with a conical spiral one with the same length and cross-section, the Nusselt number would be increased by 150%. On the other hand, the pressure drop would increase by 30%. For a circular cross-section with a similar condition, the increase in Nusselt number and pressure drop is 162% and 35%, respectively.
- For the isothermal boundary condition and Re=400, if a straight squared duct is replaced with a conical spiral one with the same length and cross-section, the Nusselt number would increase by 140%. For a circular cross-section with similar conditions, the increase in Nusselt number is 180%.
- The Nusselt number is highly dependent on the Reynolds number and thermal boundary condition. This is in contrast with the straight duct case in which in a fully developed region the Nusselt number is a constant.
- In constant the heat flux boundary condition, a 100-unit increase in Reynolds number in laminar and turbulent regime would result in a 0.9-unit increase in the Nusselt number. In the isothermal boundary condition, a 100-unit increase in Reynolds number in laminar and turbulent regime would result in a 0.65-unit increase in Nusselt number.
- The crossflow effect has an impact on temperature distribution in laminar flow but it has almost no effect in a turbulent flow.
- The use of nanofluid would enhance the average temperature of each section. Heat could be more diffused to the center of the pipe when nanoparticles are added to the coolant.
- In the isothermal boundary condition, the addition of nanoparticles up to 4% (weight fraction), would cause the heat transfer rate to increase by 4%, 5.5%, and 1.8% for CuO/water, Cu/Water, and CNT water, respectively.
- In the constant heat flux boundary condition, the addition of nanoparticles up to 4% (weight fraction), would cause wall temperature to decrease by 7.5%, 8.0%, and 3.5% for CuO/water, Cu/Water, and CNT water, respectively.
- The addition of nanoparticles up to 4% (weight fraction), would cause wall pressure drop to increase by 17%, 24%, and 10% for CuO/water, Cu/Water, and CNT water, respectively.

References

[1] Saha, S.K., Tiwari, M., Sundén, B., Wu, Z., "Advances in heat transfer enhancement.", ISBN: 978-3-319-29480-3, Springer International Publishing, 2016.

[2] Siddique, M., Khaled, A.A, Abdulhafiz, N. I. and Boukhary A. Y., "Recent Advances in Heat Transfer Enhancements: A Review Report", International Journal of Chemical Engineering, 2010, id.106461, pp. 475-503.

[3] Promvonge P., Pethkool S., Pimsarn M., Thianpong C., "Heat transfer augmentation in a helical-ribbed tube with double twisted tape inserts", International Communications in Heat and Mass Transfer, Elsevier, vol. 39, Issue 7, pp. 953–959, 2012

[4] Eiamsa-ard S., Nivesrangsan P., Chokphoemphun S., and Promvonge P., "Influence of combined non-uniform wire coil and twisted tape inserts on thermal performance characteristics", Int. Comm. in Heat and Mass Transfer, Vol. 37, P. 850-856, 2010.

[5] Srinivasacharya, D., K. D.G, and S. N.K, INTERNATIONAL CONFERENCE ON COMPUTATIONAL HEAT AND MASS TRANSFER (ICCHMT) - 2015Numerical Analysis and Optimization of Heat Transfer and Friction Factor in Dimpled Tube Assisted with Regularly Spaced Twisted

Tapes Using Taguchi and Grey Relational Analysis. Procedia Engineering, 2015. 127: p. 652-659.

[6] Tiwari, M. and S.K. Saha, Laminar Flow Through a Circular Tube Having Transverse Ribs and Twisted Tapes. Journal of Thermal Science and Engineering Applications, 2015. 7(4): p. 041009-041017.

[7] 7. zmi,W.H., Sharma,K.V., Mamat,R. and Anuar, S., "Turbulent Forced Convection Heat Transfer of nanofluids with Twisted Tape Insert in a Plain Tube", Energy Procedia, Elsevier, vol. 52, pp. 296–307, 2014.

[8] Nanan K, Pimsarn M, Thianpong C, Eiamsa-Ard S., "Heat transfer enhancement by helical screw tape coupled with rib turbulators", Journal of Mechanical Science and Technology., 28: 4771-4779., 2014, DOI: 10.1007/s12206-014-1044-z

[9] YAN Ke, GE Pei-qi, HU Rui-Rong, et al. Heat transfer and resistance characteristics of conical spiral tube bundle based on field synergy principle[J]. Chinese Journal of Mechanical Engineering, 2012, 25(2): 370-376.

[10] Yan J., Shamim T., Chou S. K., Li H. et al., Clean, efficient and affordable energy for a sustainable future: The 7th International Conference on Applied Energy (ICAE2015) Thermochemical Conversion of Microalgae: Challenges and Opportunities. Energy Procedia 2015, 75, 819–826.

[11] Mozafari, M., Akhavan-Behabadi, M.A., Qobadi-Arfaee, H., Fakoor-Pakdaman andM., "Condensation and pressure drop characteristics of R600a in a helical tube-in-tube heat exchanger at different inclination angles". Applied Thermal Engineering, 2015. 90: p. 571-578.

[12] Purandare, P.S., M.M. Lele, and R.K. Gupta, Investigation on thermal analysis of conical coil heat exchanger. International Journal of Heat and Mass Transfer, 2015. 90: p. 1188-1196.

[13] Hashemian, M., S. Jafarmadar, and H. Sadighi Dizaji, A comprehensive numerical study on multi-criteria design analyses in a novel form (conical) of double pipe heat exchanger. Applied Thermal Engineering, 2016. 102: p. 1228-1237.

[14] Mami-Meibodi, Anvari, Javaherdeh, and Rashidi, "Numerical and experimental investigation of heat transfer behavior in a round tube with the special conical ring inserts," Energy Conversion and Management, vol. 88, pp. 214–217, 2014.

[15] Raja, M. / Vijayan, R. / Dineshkumar, P. / Venkatesan, M., "Review on nanofluids characterization, heat transfer characteristics and applications", Renewable and Sustainable Energy Reviews, 2016. 64: p. 163-173.

[16] Vanaki, S.M., P. Ganesan, and H.A. Mohammed, Numerical study of convective heat transfer of nanofluids: A review. Renewable and Sustainable Energy Reviews, 2016. 54: p. 1212-1239.

[17] Purandare, P.S., M.M. Lele, and R.K. Gupta, Experimental investigation on heat transfer analysis of conical coil heat exchanger with 90° cone angle. Heat and Mass Transfer, 2015. 51(3): p. 373-379.

[18] Muhammad, Mahmud Jamil, Muhammad, Isa Adamu, Sidik, Nor Azwadi Che, Yazid, Muhammad Noor Afiq Witri, "The use of nanofluids for enhancing the thermal performance of stationary solar collectors: A review.", Renewable and Sustainable Energy Reviews, 2016. 63: p. 226-236.

[19] Sun, Bin; Peng, Cheng; Zuo, Ruiliang; Yang, Di; Li, Hongwei, "Investigation on the flow and convective heat transfer characteristics of nanofluids in the plate heat exchanger.", Experimental Thermal and Fluid Science, 2016. 76: p. 75-86.

[20] Xia, G.D., Liu, R., Wang, J. and Du, M., "The characteristics of convective heat transfer in microchannel heat sinks using Al2O3 and TiO2 nanofluids.", International Communications in Heat and Mass Transfer, 2016. 76: p. 256-264.

[21] Abbassi, Y., A.S. Shirani, and S. Asgarian, Two-phase mixture simulation of Al2O3/water nanofluid heat transfer in a non-uniform heat addition test section. Progress in Nuclear Energy, 2015. 83: p. 356-364.

[22] Abbassi, Y., Talebi, M., Shirani, A.S., Khorsandi, J., "Experimental investigation of TiO2/Water nanofluid effects on heat transfer characteristics of a vertical annulus with non-uniform heat flux in a non-radiation environment", Annals of Nuclear Energy, 2014. 69: p. 7-13.

[23] Waghole, D. R., Warkhedkar, R. M., Kulkarni, V. S., Shrivastva, R. K., "Studies on heat transfer in flow of silver nanofluid through a straight tube with twisted tape inserts", Heat and Mass Transfer, 2016. 52(2): p. 309-313.

[24] Sasmito, A.P., J.C. Kurnia, and A.S. Mujumdar, Numerical evaluation of laminar heat transfer enhancement in nanofluid flow in coiled square tubes. nanoscale Research Letters, 2011. 6(1): p. 1-14.

[25] Gautam, PK., Verma, AK., Maheshwar, S. and Singh, TN., Thermomechanical analysis of different types of sandstone at elevated temperature, Rock Mechanics and Rock Engineering, 2016, 49 (5), 1985-1993

[26] Manish Kumar Jha, Verma, AK. and Maheshwar, Sachin, Study of temperature effect on thermal conductivity of Jhiri shale from Upper Vindhyan, India, Bulletin of Engineering Geology and the Environment,2016, 1-12

[27] Dutt, A., Saini, MS., Singh, TN., Verma, AK. and Bajpai, RK., Analysis of thermo-hydrologic-mechanical impact of repository for high-level radioactive waste in clay host formation: an Indian reference disposal system, EnvironmentalEarth Sciences,2012, 66 (8), 2327-2341

[28] Masoumi, N., N. Sohrabi, and A. Behzadmehr, A new model for calculating the effective viscosity of nanofluids. Journal of Physics D: Applied Physics, 2009. 42(5): pp. 255305-255310.

[29] Chon, C.H., Kihm, K.D., Lee, S.P. and Choi, S.U.S., "Empirical correlation finding the role of temperature and particle size for nanofluid (Al2O3) thermal conductivity enhancement", Applied Physics Letters 87 (15) (2005) 153107–153110.

[30] Bejan, A., "Convection heat transfer.", ISBN: 978-0-470-90037-6, WILEY, 2013.

[31] Çengel, Y.A., Heat and mass transfer: a practical approach. 2007, Boston: McGraw-Hill.

[32] Manlapaz, R.L. and S.W. Churchill, FULLY DEVELOPED LAMINAR CONVECTION FROM A HELICAL COIL. Chemical Engineering Communications, 1981. 9(1-6): p. 185-200.

[33] Bejan, A., Kraus, A.D., "Heat transfer handbook.", ISBN: 978-0-471-39015-2. WILEY, 2003.

[34] Palanisamy,K., Mukesh kumar,P. C., "Heat Transfer Enhancement and Pressure Drop Analysis of a Cone Helical Coiled Tube Heat Exchanger using MWCNT/Water nanofluid", Journal of Applied Fluid Mechanics, 2017, Vol. 10, Special Issue, pp. 7-13.